# Magnetism, half-metallicity and electrical transport properties of V- and Cr-doped semiconductor SnTe: A theoretical study

Y. Liu, S. K. Bose, and J. Kudrnovský

Citation: Journal of Applied Physics **114**, 213704 (2013); doi: 10.1063/1.4838076
View online: http://dx.doi.org/10.1063/1.4838076
View Table of Contents: http://scitation.aip.org/content/aip/journal/jap/114/21?ver=pdfcov
Published by the AIP Publishing

# Magnetism, half-metallicity and electrical transport properties of V- and Cr-doped semiconductor SnTe: A theoretical study

Y. Liu,[1] S. K. Bose,[2] and J. Kudrnovský[3]
[1]*State Key laboratory of Metastable Materials Science & Technology and College of Science, Yanshan University, Qinhuangdao, Hebei 066004, China*
[2]*Physics Department, Brock University, St. Catharines, Ontario L2S 3A1, CANADA*
[3]*Institute of Physics, Academy of the Sciences of the Czech Republic, Na Slovance 2, 182 21 Prague 8, Czech Republic*

(Received 8 October 2013; accepted 16 November 2013; published online 5 December 2013)

This work presents results for the electronic structure, magnetic properties, and electrical resistivity of the semiconductor SnTe doped with 3*d* transition metals V and Cr. From the standpoint of potential application in spintronics, we look for half-metallic states and analyze their properties in both rock salt and zinc blende structures using *ab initio* electronic structure methods. In both cases, it is the Sn-sublattice that is doped with the transition metals, as has been the case with experiments performed so far. We find four half-metallic compounds at their optimized cell volumes. Results of exchange interactions and the Curie temperature are presented and analyzed for all the relevant cases. Resistivity calculation based on Kubo-Greenwood formalism shows that the resistivities of these alloys due to transition metal doping of the Sn-sublattice may vary, in most cases, from typical liquid metal or metallic glass value to 2–3 times higher. 25% V-doping of the Sn-sublattice in the rock salt structure gives a very high resistivity, which can be traced to high values of the lattice parameter resulting in drastically reduced hopping or diffusivity of the states at the Fermi level. © *2013 AIP Publishing LLC*. [http://dx.doi.org/10.1063/1.4838076]

## I. INTRODUCTION

Many of IV-VI semiconductors are found in the rock-salt structure, and are among the most interesting materials in solid state physics. These materials have small gaps which are usually less than 0.5 eV, hence they are good candidates for applications in thermoelectric devices, and infrared lasers and detectors. Among these IV-VI materials, both lead and germanium chalcogenides seem to have been studied more extensively than SnTe.[1] In recent years, SnTe thin films doped with Mn have received some attention from experimentalists interested in the magnetic order effects such as ferromagnetism and spin glass phase, and anomalous Hall effect.[2–4] Recently, SnTe-based superlattices exhibited a hole mobility of 2720 $cm^2/V\,s$, which is the highest value for any semiconductor material at room temperature was reported.[5]

The doping levels of transition metals considered so far in SnTe are small, so that magnetism arises as a percolation effect among the magnetic atoms and the substance behaves as a dilute magnetic semiconductor. Also, the only magnetic dopant considered so far appears to be Mn.[6–9] The only other dopant considered was nonmagnetic Pb.[10] This alloy system has been studied by several groups both theoretically and experimentally. In this work, we study the effect of high level doping of the Sn sublattice with magnetic atoms Cr and V, so that the electronic structure deviates strongly from that of the parent compound SnTe. In particular, we are interested in the possibility of half-metallicity in such systems. The case of low level doping, including that with Mn, will be considered in a separate work. Our theoretical cohesive energy calculations show that these are negative when either the Sn-sublattice or the Te-sublattice is doped with Cr and V at a level of 25% and higher. This implies that it should be experimentally possible to dope with transition metals such Cr- and V on either of the two sublattices. Since experimental investigations so far have been devoted to doping of the Sn-sublattice, we have narrowed our search for half-metallic states to the doping of the Sn-sublattice only. Half-metallicity[11,12] is a much sought-after property of materials from the viewpoint of their application in spintronic devices.[13] Both ferromagnetic (FM) and antiferromagnetic (AFM)[14] half-metals are of potential interest. Note that in their elemental states both V and Cr crystallize in bcc structure, with Cr being AFM and V nonmagnetic.

The most commonly occurring structure for both bulk and thin films of these compounds is the NaCl or the rock-salt (RS) structure. However, from the theoretical viewpoint, an equally interesting structure to study is the zinc blende (ZB) structure. Both RS and ZB are fcc-based, but differ in terms of the distance between the Sn and Te atoms. Irrespective of whether it is the Te- or the Sn-sublattice which is doped with 3*d* magnetic atoms, the magnetic effects should differ due to different levels of hybridization between the 3*d* orbitals and the *s* and *p* orbitals of the Sn or Te atoms. Experimentally it may be possible to grow both RS and ZB structures, even though the ground state structure appears to be RS. Thus, we have studied the electronic and magnetic properties of both these structures for different concentrations of the V, and Cr, atoms. We have employed supercell method as well as the coherent potential approximation (CPA) to study the effect of doping at various concentrations. The supercell calculations are carried out using the full potential linear augmented plane wave (FP-LAPW) method

 

using the WIEN2k code.[15] The CPA calculations are carried out within the frame-work of the tight-binding linear muffin-tin orbital (TB-LMTO) method using the atomic sphere approximation (ASA).[16,17] Thus, the FP-LAPW calculations are for doped but ordered alloys and the TB-LMTO calculations are for partially ordered alloys, with disorder in the V- or Cr-doped Sn sublattice. To distinguish them, we have used the notation $Sn_{4-x}X_xTe_4$ with $x = 1, 2, 3, 4$, where X stands for transition metal (TM) atoms, V and Cr for the wien2k supercell results, and $Sn_{1-x}X_xTe$ ($0 \leq x \leq 1$) for the TB-LMTO results. For those cases, where half-metallicity is predicted on the basis of the LAPW supercell calculations, we have calculated the exchange interaction using the linear response and multiple scattering Geen's function method implemented in the TB-LMTO basis.

## II. COMPUTATIONAL DETAILS

The crystal structures of the ternary SnTe-based compounds $Sn_{4-x}X_xTe_4$ were constructed from the unit cell of RS and ZB structures as follows. The doping levels of $x = 0.25$ or 0.75 were achieved by replacing the Sn atoms at the vertex site or face-center sites, respectively, of the RS/ZB unit cell, with the TM atoms. Both cases ($x = 0.25$ or 0.75) have the same space group ($Pm\bar{3}m$, or 221) for the RS structure, and ($P\bar{4}3m$, or 215) for ZB. The $x = 0.5$ doping is obtained by replacing the Sn atoms at the four compatible face-center sites. In this way we generate tetragonal structure ($P\bar{4}m2$, 115) for the ZB case and ($P4/mmm$, 123) for RS. This procedure of realizing the doping levels results in smallest unit (i.e., primitive) cells, with the highest possible symmetry. Numerous semiconductors are known to crystallize in the ZB or RS structures. As such the lattice parameters of these ternary compounds should be compatible with a large number of semiconductors.

Calculations were carried out within the framework of the density-functional theory (DFT),[18] using the WIEN2k[15] code based on the full-potential linear augmented plane wave plus local orbitals method. The generalized gradient approximation (GGA) proposed by Perdew *et al.* was used for exchange and correlation potentials.[19] We consider full relativistic effects for the core states and use the scalar-relativistic approximation for the valence states, neglecting the spin-orbit coupling. The latter is known to produce only a small effect on the density of states and the energy gaps, features of the electronic structure that are of interest in the present work. We used 3000 K points (Monkhorst-Park grid[20]) for the Brillouin-zone integration, set $Rmt * Kmax = 8.0$ and carried out the angular momentum expansion up to $l_{max} = 10$ in the muffin tins, and used $G_{max} = 12$ for the charge density. All core and valence states are treated self-consistently. Convergence with respect to basis set and k-point sampling was closely monitored. The self-consistency was assumed to have been achieved, when the integrated charge difference per formula unit, $\int |\rho_n - \rho_{n-1}| dr$, for the input and output charge densities $\rho_{n-1}$ and $\rho_n$ became less than 0.0001. In the calculation of Sn-X-Te in different structures, the muffin-tin (MT) radii were chosen to be 2.5, 2.3, and 2.5 a.u. for Sn, X (X = V, Cr) and Te atoms, respectively.

The results obtained with the FP-LAPW method for ordered alloys (supercells), while the TM-doped thin films of SnTe are partially random, in the sense that the Sn-sublattice sites are occupied randomly by Sn and TM atoms. We have studied the electronic structure of these partially random alloys using the TB-LMTO method in conjunction with the CPA.[16,17] These calculations employed exchange-correlation potential of Vosko, Wilk, and Nusair,[21] an *s*, *p*, *d*, *f* basis set, relativistic treatment of core electrons, and scalar-relativistic treatment of valence electrons. The results, particularly with respect to half-metallicity, were similar to those of the ordered alloys, apart from expected smoothing of some peaks in the density of states (DOS). The gaps values were marginally lower and can be ascribed to the differences between local density approximation (LDA) in TB-LMTO and GGA in FP-LAPW. The equilibrium lattice parameters were 2%–4% higher in TB-LMTO LDA calculations. The reason for the difference can be ascribed to several factors: different treatment of exchange-correlation, the use of ASA in the TB-LMTO method and the fact that the FP-lAPW supercell calculations are for ordered alloys, while the TB-LMTO-CPA calculations are for partially ordered alloys, with disorder in the positions of Sn and TM atoms inside the Sn-sublattice.

## III. ELECTRONIC STRUCTURE

### A. Results of supercell calculations using the FP-LAPW method

For each case, equilibrium lattice parameter was obtained by minimizing the total energy with respect to the cell volume. All electronic properties, such as the DOS, energy bands, and magnetic moments, were then calculated for the equilibrium lattice parameters. Among all the ternary TM compounds with the doping levels considered, we find 4 half-metallic (HM) cases: three V-doped cases for the RS structure; and one V-doped case for the ZB structure (see Tables I–IV). There is a small drop in the value of the equilibrium lattice parameter with increasing dopant concentration in all cases. Bulk moduli, calculated by using Birch-Murnaghan equation of state,[22] are found to increase with the doping level for V- and Cr-doping. The equilibrium lattice constants, X-Te bond lengths, and bulk moduli, magnetic moments, minority-spin gaps, and half-metallic gaps for the ternary compounds in RS structure are summarized in

TABLE I. Results obtained via the WIEN2k code for the RS compounds $Sn_{4-n}X_nTe_4$ (X = V, Cr): the equilibrium lattice constants *a*, the X-Te bond length $L_{XTe}$, bulk modulus *B*, magnetic moments per magnetic atom M $\mu_B$, minority-spin gaps $G_{MIS}$ (eV), and half-metallic gaps $G_{HM}$ (eV). All results shown are obtained using GGA (see text).

| Compounds | *a* (Å) | *L* (Å) | *B* (GPa) | $G_{MIS}$ (eV) | $G_{HM}$ (eV) |
|---|---|---|---|---|---|
| $Sn_3V_1Te_4$ | 6.2608 | 3.1304 | 43.1441 | 0.35 | 0.02 |
| $Sn_2V_2Te_4$ | 6.0837 | 3.0418 | 47.4565 | 0.44 | 0.06 |
| $Sn_1V_3Te_4$ | 5.9096 | 2.9548 | 56.1428 | 0.38 | 0.05 |
| $Sn_3Cr_1Te_4$ | 6.2641 | 3.1321 | 42.9614 | – | – |
| $Sn_2Cr_2Te_4$ | 6.0931 | 3.0465 | 46.8871 | – | – |
| $Sn_1Cr_3Te_4$ | 5.9154 | 2.9577 | 54.7236 | – | – |

TABLE II. Magnetic moment per magnetic atom (f.u.) in units of bohr magneton $\mu_B$, for the RS compounds $Sn_{4-n}X_nTe_4$ (X = V, Cr), at their respective equilibrium volumes, obtained by using the FP-LAPW method (WIEN2k). Moments associated with X, Te, Sn muffin-tin spheres and the interstitial region (Int) are shown separately.

| Compounds | X ($\mu_B$) | Te ($\mu_B$) | Sn ($\mu_B$) | Int ($\mu_B$) | Tot ($\mu_B$) |
|---|---|---|---|---|---|
| $Sn_3V_1Te_4$ | 2.674 | −0.068 | −0.001 | 0.505 | 3.000 |
| $Sn_2V_2Te_4$ | 2.644 | −0.147 | −0.008 | 0.511 | 3.000 |
| $Sn_1V_3Te_4$ | 2.607 | −0.171 | −0.019 | 0.510 | 3.000 |
| $Sn_3Cr_1Te_4$ | 3.733 | −0.072 | −0.006 | 0.553 | 4.029 |
| $Sn_2Cr_2Te_4$ | 3.680 | −0.075 | −0.016 | 0.548 | 4.011 |
| $Sn_1Cr_3Te_4$ | 3.622 | −0.113 | −0.025 | 0.549 | 4.003 |

TABLE III. Results obtained via the WIEN2k code for the ZB compounds $Sn_{4-n}X_nTe_4$ (X = V, Cr): the equilibrium lattice constants $a$, the X-Te bond length $L_{XTe}$, bulk modulus $B$, magnetic moments per magnetic atom M $\mu_B$, minority-spin gaps $G_{MIS}$ (eV), and half-metallic gaps $G_{HM}$ (eV). All results shown are obtained using GGA (see text).

| Compounds | a (Å) | L (Å) | B (GPa) | $G_{MIS}$ (eV) | $G_{HM}$ (eV) |
|---|---|---|---|---|---|
| $Sn_3V_1Te_4$ | 6.9768 | 3.0211 | 23.9285 | … | – |
| $Sn_2V_2Te_4$ | 6.7059 | 2.9040 | 29.3370 | … | – |
| $Sn_1V_3Te_4$ | 6.4471 | 2.7917 | 36.3632 | 0.67 | 0.12 |
| $Sn_3Cr_1Te_4$ | 6.9799 | 3.0224 | 42.9614 | … | – |
| $Sn_2Cr_2Te_4$ | 6.7105 | 2.9057 | 29.6065 | … | – |
| $Sn_1Cr_3Te_4$ | 6.4639 | 2.7989 | 36.2736 | | |

TABLE IV. Magnetic moment per magnetic atom (f.u.) in units of bohr magneton $\mu_B$, for the ZB compounds $Sn_{4-n}X_nTe_4$ (X = V, Cr), at their respective equilibrium volumes, obtained by using the FP-LAPW method (WIEN2k). Moments associated with X, Te, Sn muffin-tin spheres, and the interstitial region (Int) are shown separately.

| Compounds | X ($\mu_B$) | Te($\mu_B$) | Sn($\mu_B$) | Int($\mu_B$) | Tot($\mu_B$) |
|---|---|---|---|---|---|
| $Sn_3V_1Te_4$ | 2.764 | −0.084 | −0.001 | 0.595 | 3.022 |
| $Sn_2V_2Te_4$ | 2.696 | −0.120 | −0.010 | 0.609 | 3.055 |
| $Sn_1V_3Te_4$ | 2.576 | −0.123 | −0.016 | 0.593 | 3.000 |
| $Sn_3Cr_1Te_4$ | 3.853 | −0.082 | −0.007 | 0.659 | 4.163 |
| $Sn_2Cr_2Te_4$ | 3.759 | −0.126 | −0.022 | 0.675 | 4.159 |
| $Sn_1Cr_3Te_4$ | 3.666 | −0.112 | 0.029 | 0.703 | 4.230 |

Tables I and II. The same quantities for the ternary compounds in ZB structure are summarized in Tables III and IV.

Note that in all cases studied and reported in Tables I, the RS structure has lower energy than the ZB, indicating the equilibrium bulk phase to be RS at low temperatures. However, it might be possible to grow thin films of these compounds in ZB structure under suitable conditions. Therefore, there is some merit in comparing the magnetic properties of these two fcc-based phases.

The DOS of these ordered compounds at their equilibrium lattice parameters are shown in Figs. (1–4). Majority and minority spin DOS are shown as spin up and down, respectively. These results clearly show in which cases half-metallicity is most robust, i.e., the Fermi level is most widely separated from the band edges. The partial atom-projected DOS show that the states at the Fermi level have a high TM character, with the amount of the TM character changing

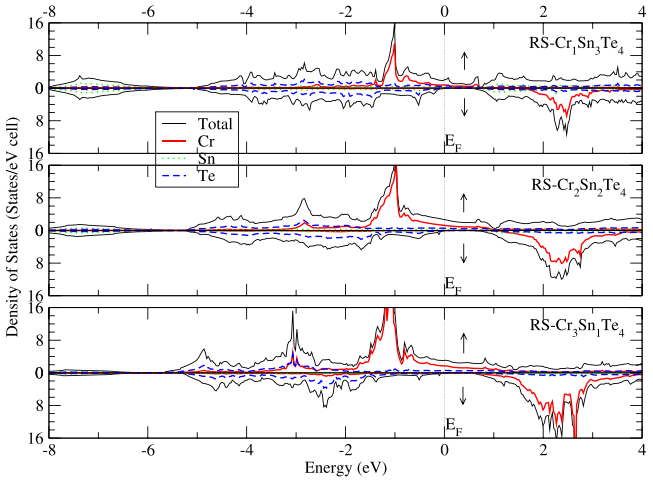


FIG. 1. Densities of states in Cr-doped SnTe alloys in RS structure.

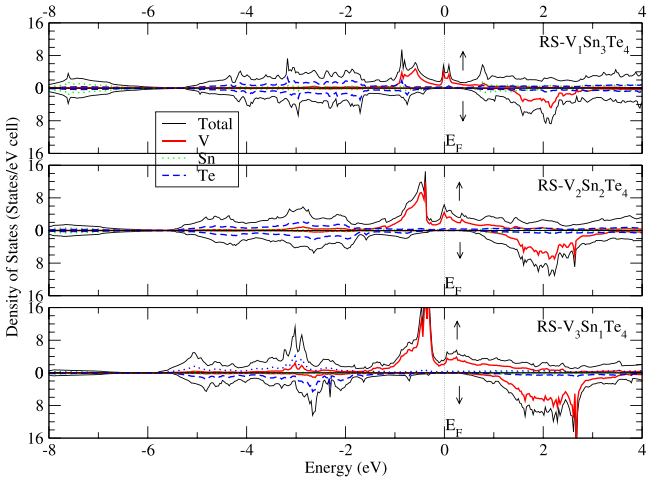


FIG. 2. Densities of states in V-doped SnTe alloys in RS structure.

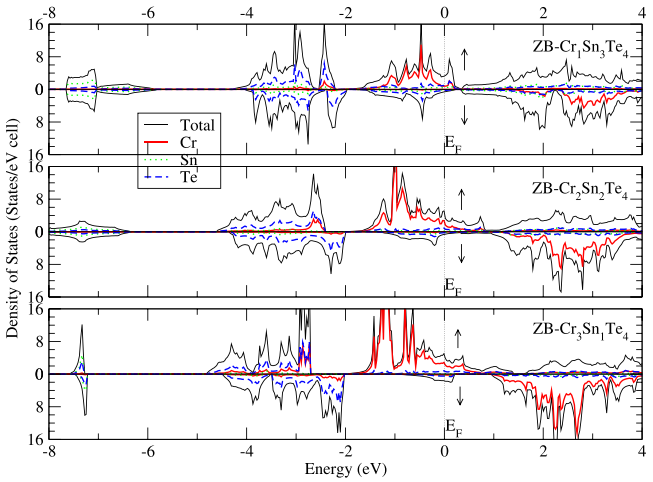


FIG. 3. Densities of states in Cr-doped SnTe alloys in ZB structure.

with TM concentration. Table I shows the actual HM alloys. In spite of the appearance, none of the Cr-doped cases is a pure HM, although the degree of spin polarization is very high. This is shown in Fig. 5, where the minority spin DOS (shown as spin down) are displayed on an expanded scale for

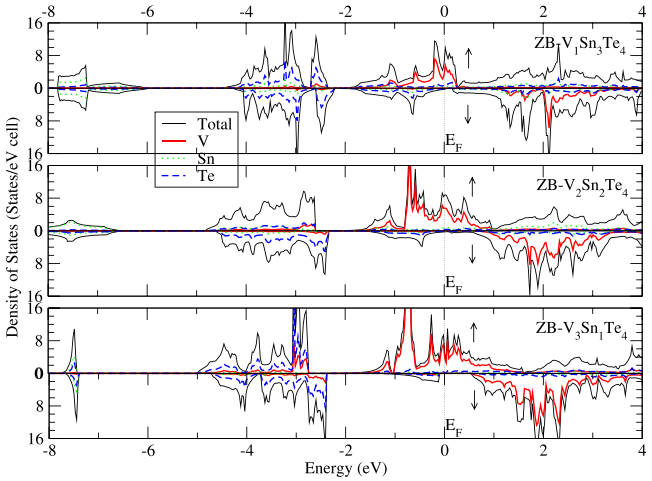


FIG. 4. Densities of states in V-doped SnTe alloys in ZB structure.

Cr-doped RS case. The densities of states are very low, but clearly nonzero. The same is true for ZB $Sn_2V_2Te$.

## IV. EXCHANGE INTERACTION AND CURIE TEMPERATURE

*First-principles* calculations of the thermodynamic properties of itinerant magnetic systems, via mapping[23,24] of the zero temperature band energy onto a classical Heisenberg model

$$H_{\text{eff}} = -\sum_{i,j} J_{ij}\, \mathbf{e}_i \cdot \mathbf{e}_j\,, \tag{1}$$

have been discussed in detail in our previous publications.[25,26] Here $i$, $j$ are site indices, $\mathbf{e}_i$ is the unit vector pointing along the direction of the local magnetic moment at site $i$, and $J_{ij}$ is the exchange interaction between the moments at sites $i$ and $j$. The calculations are based on a mapping procedure due to Liechtenstein *et al.*[27–29] The method was later extended to random magnetic systems by Turek *et al.*, using CPA and the TB-LMTO method.[30] The exchange integral in Eq. (1) is given by

$$J_{ij} = \frac{1}{4\pi} \lim_{\epsilon \to 0^+} Im \int tr_L \left[\Delta_i(z) g_{ij}^{\uparrow}(z) \Delta_j(z) g_{ji}^{\downarrow}\right] dz, \tag{2}$$

where $z = E + i\epsilon$ represents the complex energy variable, $L = (l,\ m)$, and $\Delta_i(z) = P_i^{\uparrow}(z) - P_i^{\downarrow}(z)$, representing the difference in the potential functions for the up and down spin electrons at site "$i$". $g_{ij}^{\sigma}(z)(\sigma = \uparrow, \downarrow)$ represents the matrix elements of the Green's function of the medium for the up and down spin electrons. For sublattices with disorder, this is a configurationally averaged Green's function, obtained via using the prescription of CPA. It should be noted that the spin magnetic moments are included in the above definition of $J_{ij}$. Positive and negative values of $J_{ij}$ imply FM and AFM couplings, respectively, between the atoms at sites $i$ and $j$. In the above procedure outlined by Liechtenstein *et al.*,[27–29] exchange interactions are calculated by considering spin deviation from a reference state. Negative exchange interactions resulting from calculations based on a FM reference state would suggest instability of the assumed FM ground state. With this mind, we have computed the exchange interactions for the most interesting cases, i.e., those promising robust HM states.

The results in Tables I and III show that the HM state occurs mostly in the RS structure and for V-doping. In Figs. 6–8, we show results for the cases with 75%, 50%, and 25% doping with V, respectively, for the RS structure. All of these cases show HM character. Calculations of exchange interactions were carried out for both FM and disordered local moment (DLM) reference states. This was necessary, since although the exchange interactions between the V atoms were found to be antiferromagnetic (i.e., negative) for the FM reference state, the interactions among the Sn- and V-atoms were non-negligible and so were those between V-atoms and empty spheres (required by ASA for space-filling). Some of these interactions were found to be ferromagnetic (positive). These interactions appear as a result of induced moments on the nonmagnetic atoms and the empty spheres. These induced moments disappear for the DLM reference state, where only the robust moment of the magnetic atom stays non-zero. Within the Stoner model, a nonmagnetic state above the Curie temperature $T_c$ is characterized

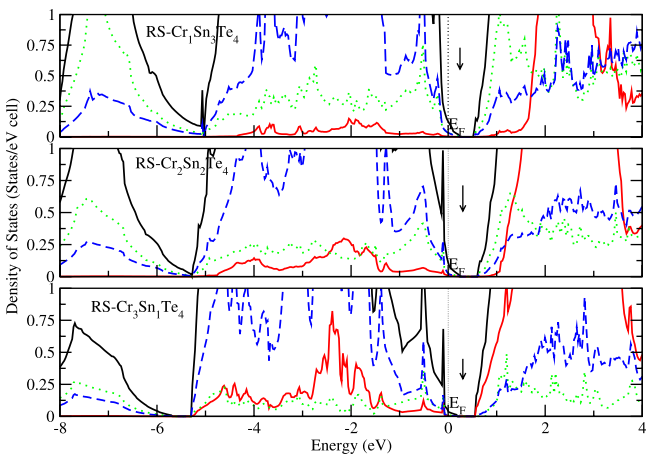


FIG. 5. Minority spin densities of states in Cr-doped SnTe alloys in RS structure.

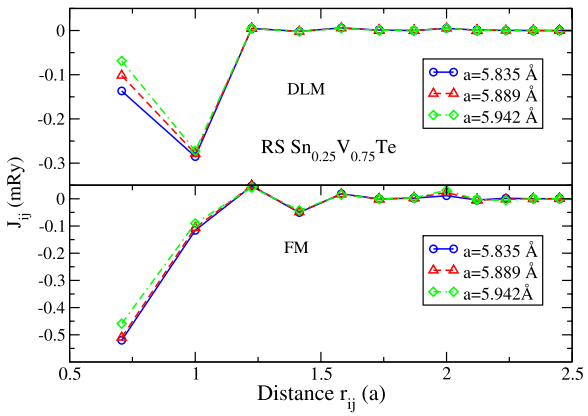


FIG. 6. Exchange interaction between the V-atoms in RS $Sn_{0.25}V_{0.75}Te$ as a function of interatomic distance, expressed in units of lattice parameter $a$, for DLM (upper panel) and FM (lower panel) reference states. WIEN2k equilibrium value of a = 5.9096 Å.

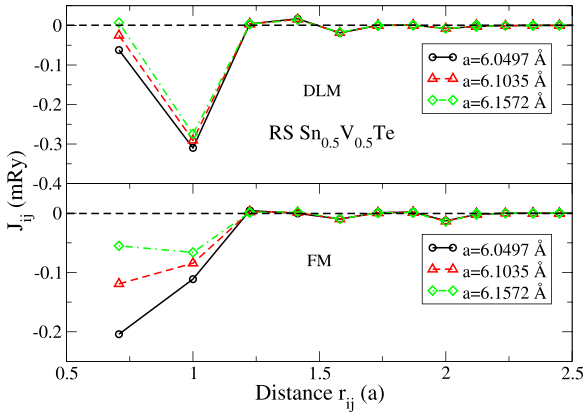


FIG. 7. Exchange interaction between the V atoms in RS $Sn_{0.50}V_{0.50}Te$ as a function of interatomic distance, expressed in units of lattice parameter $a$, for DLM (upper panel) and FM (lower panel) reference states. WIEN2k equilibrium value of a = 6.0837 Å.

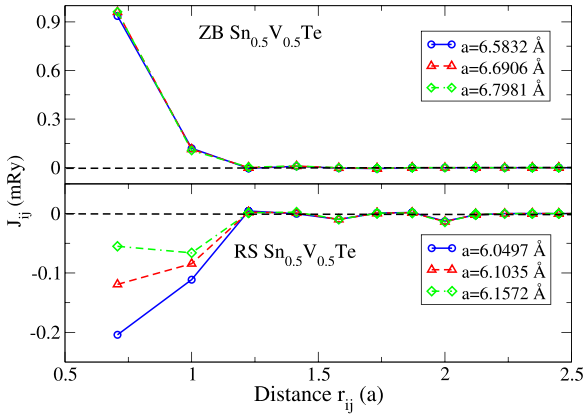


FIG. 9. Comparison of the exchange interaction between the V atoms in ZB and RS $Sn_{0.50}V_{0.50}Te$ as a function of interatomic distance expressed in units of lattice parameter $a$. Reference state is chosen as FM. WIEN2k ZB and RS equilibrium values of $a$ are 6.7059 Å and 6.2608 Å, respectively.

by the vanishing of the local moments in magnitude, which costs considerably more energy than is needed to disorder the local moments, leading to a state of zero net magnetization. In the DLM model,[31,32] the nonmagnetic state is described as one where the local moments remain nonzero in magnitude above $T_c$, but disorder in their direction above $T_c$ causes global magnetic moment to vanish. Within the collinear moment formulation, where all local axes of spin-quantization point in the same direction, DLM can be treated as a binary alloy problem[25] with 50% of the moments pointing in a direction opposite to the rest, the magnitudes of all moments being the same. Figs. 6–8 show that the AFM interactions between the V atoms persist in the DLM state, although somewhat reduced in magnitude. For 75% V, for the FM reference state the magnetic moments per cell are found to be ~2.9–3.0 $\mu_B$ for the curves shown in Fig. 6, while the numbers for the DLM state are ~2.6–2.7 $\mu_B$. Similar results follow for the other two cases shown in Figs. 7 and 8. The strength of the AFM interactions weakens with the decrease in V-concentration. The fact that the magnitude of the moment is not drastically reduced in the DLM state from its FM state value points to the validity of the Heisenberg model description adopted in this work.

In contrast to the RS structure, the ZB structure appears to promote FM interactions. We illustrate this in Fig. 9, where the exchange interactions between the V-atoms for the FM reference state are compared for $Sn_{0.5}V_{0.5}Te$ in RS and ZB structures. The lattice parameter values are around the equilibrium values given by FP-LAPW WIEN2k code, varying from below to above. According to Table III, this material is not HM, but the situation persists for $Sn_{0.25}V_{0.75}Te$, which does show HM gap (for both RS and ZB structures). The ZB structure gives a FM $Sn_{0.25}V_{0.75}Te$, while the corresponding RS compound is AFM (Fig. 10). Fig. 9 illustrates the point that with increasing distance between the V and Te atoms in the RS structure, i.e, with decreasing hybridization of the $d$-orbitals of V with the $s$- and $p$-orbitals of Te, the AFM exchange interactions between the V atoms decrease in magnitude. With increasing lattice parameter, the overlap of the neighboring $d$-orbitals of V also decreases. This has the effect of the V-V interaction to grow towards FM. This is further increased in the ZB phase with much larger lattice parameter, where the V-V interactions are not only FM, but also seem to have saturated. These trends are also reflected in Fig. 10.

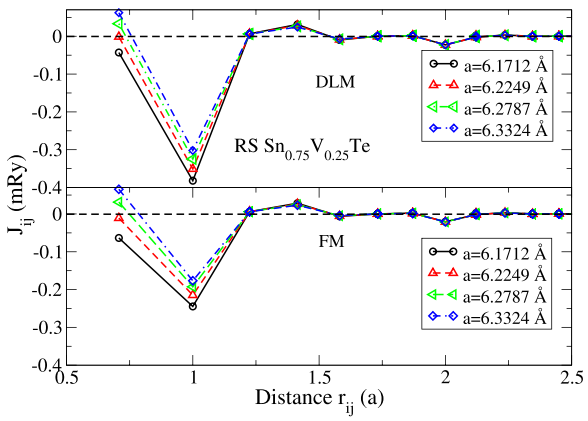


FIG. 8. Exchange interaction between the V atoms in RS $Sn_{0.75}V_{0.25}Te$ as a function of interatomic distance, expressed in units of lattice parameter $a$, for DLM (upper panel) and FM (lower panel) reference states. WIEN2k equilibrium value of a = 6.2608 Å.

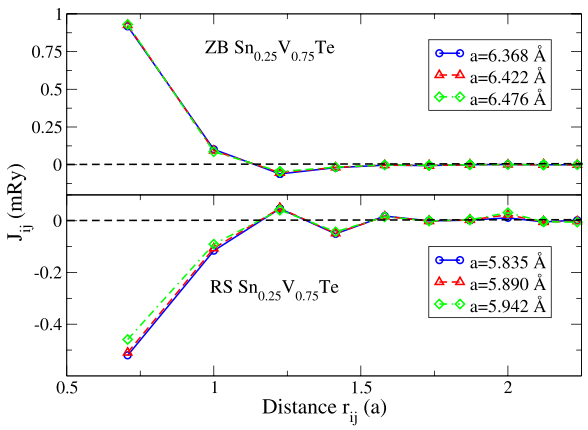


FIG. 10. Comparison of the exchange interaction between the V atoms in ZB and RS $Sn_{0.25}V_{0.75}Te$ as a function of interatomic distance expressed in units of lattice parameter $a$. Reference state is chosen as FM. Equilibrium lattice parameter values are given in Tables I and III.

Even though we did not find any HM case for Cr-doped SnTe, it is important to point out that such materials would be overwhelmingly FM. In Fig. 11, we show the exchange interactions in both ZB and RS structures for $Sn_{0.5}Cr_{0.5}Te$, with lattice parameters around the LAPW equilibrium values. The results shown are for FM reference state.

From the viewpoint of spintronic devices, both FM and AFM HM materials are of potential interest. The ideal case is a HM AFM material, which is a fully compensated ferrimagnet. Such a compound should be insensitive to external magnetic field, and unlike a ferromagnet, would not bring in stray flux. As a result, devices based on these AFM HM materials are expected to consume less energy. AFM HM materials have attracted considerable attention in recent years.[33–37]

We estimate the Curie temperature $T_c$ for the ZB structure $Sn_{0.25}V_{0.75}Te$, which exhibits FM interactions among the V-atoms. We have calculated the Curie temperature $T_c$ using both the mean-field approximation (MFA) and the more accurate random-phase approximation (RPA).[38] If the magnetic sublattice consists only of the magnetic atoms X, then in the MFA, the Curie temperature is given by

$$k_B T_c^{\mathrm{MFA}} = \frac{2}{3}\sum_{i\neq 0} J_{0i}^{\mathrm{X,X}}, \tag{3}$$

where the sum extends over all the neighboring shells and involves the exchange interactions between the magnetic atoms *X*. MFA is known to grossly overestimate $T_c$. A much more improved description of finite-temperature magnetism is actually provided by the RPA. Again, if the magnetic sublattice consists only of the magnetic atoms X, then the RPA $T_c$ given by

$$(k_B T_c^{\mathrm{RPA}})^{-1} = \frac{3}{2}\frac{1}{N}\sum_{\mathbf{q}} [J^{\mathrm{X,X}}(\mathbf{0}) - J^{\mathrm{X,X}}(\mathbf{q})]^{-1}. \tag{4}$$

Here, $N$ denotes the order of the translational group applied and $J^{\mathrm{X,X}}(\mathbf{q})$ is the lattice Fourier transform of the real-space exchange interactions $J_{ij}^{\mathrm{X,X}}$. We have modified Eqs. (3) and (4) for our $Sn_{1-x}X_xTe$ alloys using virtual crystal approximation (VCA). This involves simply weighting the Tc's obtained from Eqs. (3) and (4) by the square of the concentration ($x^2$) of the X (TM) atoms. The RPA-VCA neglects the magnetic percolation effect[39–41] which is important, in particular, for the case of low concentration of magnetic atoms. Its effect is estimated to be significant for less than 20% concentration of magnetic atoms and weaker for concentrated alloys under consideration in this work. For the 25%, 50%, and 75% TM-doping of the Sn-sublattice considered, the percolation effect may lower the estimated $T_c$s somewhat, by decreasing amounts.

In the upper panel of Fig. 12, we show the variation of $T_c$ with lattice parameter in ZB structure $Sn_{0.25}V_{0.75}Te$ for values around the FP-LAPW equilibrium lattice parameter. This is the only HM case we have encountered among the various doping levels studied. For comparison, in the lower panel of the same figure, we show the $T_c$ values for $Sn_{0.50}V_{0.50}Te$. The results shown are for the FM reference states and calculated using the RPA. A problem arises in the computation of $T_c$ using either Eq. (3) or Eq. (4) when, in addition to the robust moments on the magnetic atoms, there are induced moments on apparently non-magnetic atoms, interstitial spaces or, in case of the LMTO method, empty spheres. This problem has been discussed in detail in our previous publication[25] and references cited therein. As shown by Sandratskii *et al.*,[23] the calculation of $T_c$ using RPA is considerably more involved even for the case where only one secondary induced interaction needs to be considered, in addition to the principal interaction between the strong moments. The complexity of the problem increases even for MFA, if more than one secondary interaction is to be considered. Since we are only interested in a rough estimation of $T_c$, we simply use the the RPA prescription considering only the TM moments in Eq. (4). The results further modified in the spirit of VCA, are shown in Figs. 12 and 13. Fig. 13 shows the results for the Cr-doping case to illustrate the point that Cr-doping leads to FM interactions for both ZB and RS structures. This result is consistent with our previous study for TM-doped semiconductor GeTe,[45] where the Cr-doped cases were found to be overwhelmingly FM.

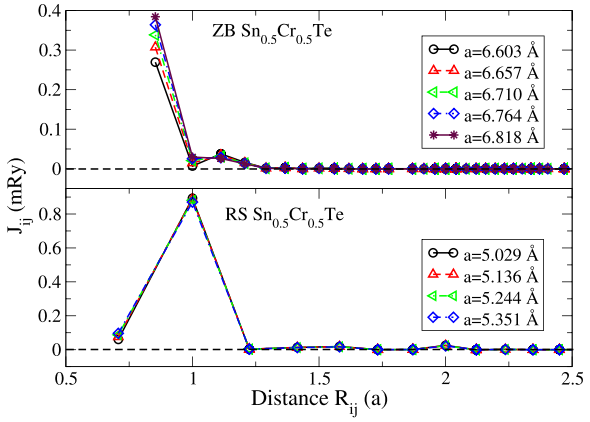


FIG. 11. Exchange interaction between the Cr atoms in ZB and RS $Sn_{0.50}Cr_{0.50}Te$ as a function of interatomic distance expressed in units of lattice parameter *a*. Reference state is chosen as FM. Equilibrium lattice parameter values are given in Tables I and III.

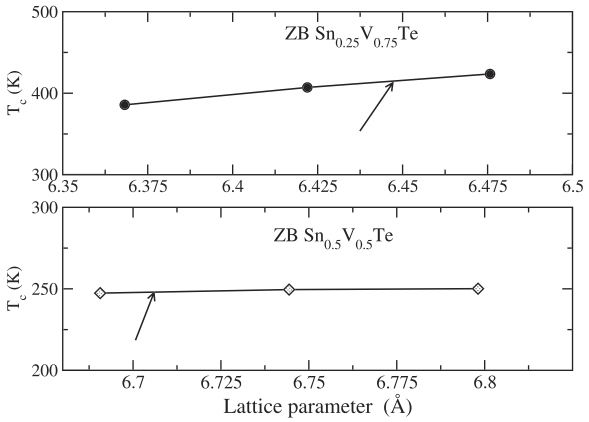


FIG. 12. $T_c$ (via RPA together with VCA) versus lattice parameter *a* in ZB $Sn_{0.25}V_{0.75}Te$. The arrow indicates the value for the equilibrium lattice parameter.

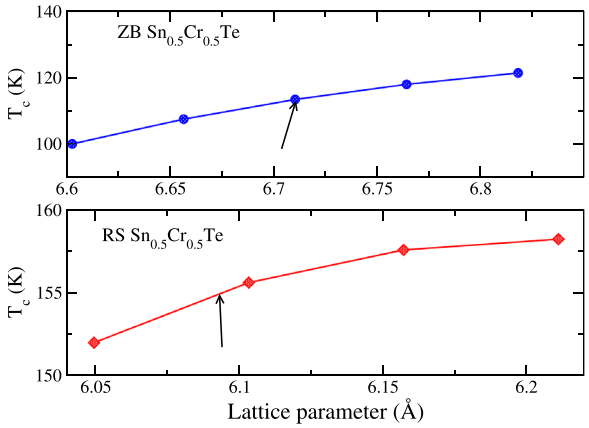


FIG. 13. $T_c$ (via RPA together with VCA) versus lattice parameter $a$ in ZB and RS $Sn_{0.50}Cr_{0.50}Te$ alloys. The arrow indicates the value for the equilibrium lattice parameter.

## V. ELECTRICAL RESISTIVITY

The residual resistivity of the half-metals was calculated by using the linear-response theory as formulated in the framework of the TB-LMTO-CPA method and the Kubo-Greenwood (K-G) formalism.[42,43] Within the K-G formalism, transport properties, such as conductance or conductivity at the energy $E$: $\sigma(E)$, can be expressed in the form

$$\sigma(E) \propto Tr\{\delta(E-H)J\delta(E-H)J\}, \tag{5}$$

where $J$ is the velocity or current operator. The physical conductivity is obtained by setting $E = E_F$. The velocity/current operator can be related, via the Heisenberg equation of motion, to the commutator of the Hamiltonian $H$ and the position operator $x$ (with $e = \hbar = 1$)

$$J = -i[x, H]. \tag{6}$$

The Dirac delta functions appearing in Eq. (5) can be related to the imaginary part of the Green's function $G(E - H)$. The representation of the Green's function and the evaluation of the matrix elements of $J$ in the TB-LMTO basis have been discussed in detail in Refs. 42 and 43. Since the equilibrium lattice parameters given by the TB-LMTO method are slightly different from those given by the FP-LAPW scheme, we have considered a few lattice parameter values around the FP-LMTO equilibrium values. As mentioned earlier, the differences in the equilibrium lattice parameter values are not only due to the differences in the two methods and the exchange-correlation potentials used, but also due to the fact that the FP-LAPW values are for ordered alloys and the TB-LMTO values are for partially ordered alloys (with disorder in the Sn-sublattice). The calculated resistivity originates from the disorder in the Sn-sublattice due to the TM dopant atom. The purpose of this study is to get estimates of the resistivity of these alloys in relation to other disordered metallic systems such as metallic glasses and liquid metals. The results are summarized in Table V. The metallic character of the system increases with the TM dopant concentration. The resistivity decreases with increasing DOS at the Fermi level as well as decreasing lattice parameter. The latter should result in increased hopping, i.e., increased diffusivity of the states at the Fermi level. For the RS systems, the resistivity of the 25% V-doping case is very high compared with that of a typical liquid metal or a metallic glass, which is around 150–200 $\mu\Omega$ cm. This is partly due to high value of the lattice parameter, resulting in reduced hopping between neighboring sites in general and partly due to the high value of the local moment on V atoms, giving rise to high magnetic scattering. Of course the high value of the moment itself can be traced to increased lattice parameter and reduced co-ordination with respect to elemental solid V, which is nonmagnetic. With increasing V-concentration, the lattice parameter as well as the local moment on V-atoms decreases and the resistivity comes down, decreasing by a factor of 10% or more by the time 50% V-doping is reached. For 75%-V, the resistivity is in the typical liquid/glassy metal range. For the 75% V-doped ZB alloy, the resistivity is somewhat increased with respect to the corresponding RS structure value, mainly due to the increased lattice parameter. In addition, at these high values of the lattice parameter, resistivity appears to have reached saturation with respect to small lattice parameter variation. The calculated resistivities are all for the magnetic or low temperature phase. For comparison, we have also included the ZB $Sn_{0.50}V_{0.50}Te$ alloys as the last entry. This compound is not a half-metal, but almost so with a very high degree of spin polarization. As a result, its resistivity is not drastically different from that of the HM compound ZB $Sn_{0.25}V_{0.75}Te$,

TABLE V. Resistivity $\rho$ of the RS and ZB HM compounds in units of $\mu\Omega$ cm, as computed by using the Kubo-Greenwood formalism. Calculations were done for a few lattice parameter values $a$ around the Wien2k equilibrium values (Tables I and III) of the corresponding ordered alloys, shown in parentheses beside the compound name. Resistivity values for the corresponding lattice parameters are shown.

| Compounds | $a$(Å) | $\rho(\mu\Omega$ cm) |
|---|---|---|
| RS $Sn_{0.75}V_{0.25}Te$ (6.2608 Å): | | |
| | 6.171185 | 3724.90 |
| | 6.224923 | 4113.53 |
| | 6.278661 | 4482.32 |
| | 6.332398 | 4829.87 |
| RS $Sn_{0.50}V_{0.50}Te$ (6.0837 Å): | | |
| | 6.049738 | 359.57 |
| | 6.103477 | 374.55 |
| | 6.157214 | 389.53 |
| RS $Sn_{0.25}V_{0.75}Te$ (5.9096 Å): | | |
| | 5.834789 | 130.19 |
| | 5.888526 | 143.58 |
| | 5.942264 | 183.35 |
| ZB $Sn_{0.25}V_{0.75}Te$ (6.4471 Å): | | |
| | 6.368232 | 239.86 |
| | 6.421969 | 241.11 |
| | 6.475707 | 243.06 |
| | 6.529445 | 245.65 |
| ZB $Sn_{0.50}V_{0.50}Te$ (6.7059 Å): | | |
| | 6.583182 | 371.11 |
| | 6.690657 | 394.46 |
| | 6.744394 | 402.54 |
| | 6.798131 | 411.06 |

being somewhat higher in accordance with the Nordheim[44] rule.

## VI. SUMMARY OF RESULTS AND CONCLUSIONS

Via *first-principles* calculations, we have examined the possibility of HM states in bulk $Sn_{1-x}TM_xTe$ alloys, with TM being the transition metals V, and Cr. In their elemental forms, V and Cr both crystallize in bcc structures, and while Cr is AFM, V is nonmagnetic. Although the ground state structure of the above alloys is found to be RS, we have explored the possibility of half-metallicity in RS as well as the closely related ZB structures. It is hoped that with suitable substrates some of these alloys may be grown in ZB structure as well. Attempts to do so would be worthwhile if they showed promise of potential interest for spintronic and other related applications. All the cases studied are for high doping levels: 25%, 50%, and 75% doping of the Sn-sublattice with the TM atoms. Thus, the magnetic effects are due to modifications of band structure and consequent spin-polarization, and not due to percolation among the magnetic atoms as found in dilute magnetic semiconductors. We identify several HM candidates in the RS structure. Exchange calculations indicate that the ground states in these cases would be AFM or would support complex magnetic structure. 75% doping of the Sn-sublattice with V-atoms in the ZB structure does indicate FM ground state. We also find that Cr-doping overwhelmingly supports FM ground state, even though such states would most probably not be HM. The preponderance of FM state for Cr-doping in both ZB and RS structures as well as the AFM tendencies of the V-doped alloys is in line with our previous study for TM-doped semiconductor GeTe.[45] Low temperature resistivities of the HM alloys seem to vary from the typical metallic glass/liquid metal value to about 2–3 times higher in most of these cases.

## ACKNOWLEDGMENTS

Computational facilities for this work were provided by SHARCNET, Canada. The work of Y.L. was supported by the Natural Science Foundation of Hebei Province (No. *A*2011203037). J.K. acknowledges financial support from the Grant Agency of the Czech Republic (No. P204/12/0692).

[1]R. Tsu, W. E. Howard, and L. Esaki, Phys. Rev. **172**, 779 (1968).
[2]M. Escorne and A. Mauger, J. Phys. (France) **40**, 347 (1979).
[3]A. J. Nadolny, J. Sadowski, B. Taliashvili *et al.*, J. Magn. Magn. Mater. **248**, 134 (2002).
[4]K. Racka, I. Kuryliszewska, W. Dobrowolshi, Y. J. M. Broto, M. Goiran, O. Portugall, H. Rakoto, B. Raquet, V. Dugaev, E. I. Slynko, and V. E. Slynko, J. Supercond. **16**, 289 (2003).
[5]A. Ishida, T. Yamada, T. Tsuchiya, Y. Inoue, S. Takaoka, and T. Kita, Appl. Phys. Lett. **95**, 122106 (2009).
[6]C. W. H. M. Vennix *et al.*, Phys. Rev. B **48**, 3770 (1993).
[7]W. J. M. de Jonge, H. J. M. Swagten, S. J. E. A. Eltink, and N. M. J. Stoffels, Semicond. Sci. Technol. **5**, S131–S133 (1990).
[8]P. J. T. Eggenkamp *et al.*, J. Appl. Phys. **75**, 5728 (1994).
[9]M. Inoue, K. Ishi, and H. Yagi, J. Phys. Soc. Jpn. **43**, 903 (1977).
[10]J. O. Dimmock, I. Melngailis, and A. J. Strauss, Phys. Rev. Lett. **16**, 1193 (1966).
[11]W. E. Pickett and J. S. Moodera, Phys. Today **54**(5), 39 (2001).
[12]M. I. Katsnelson, V. Yu. Irkhin, L. Chioncel, A. I. Lichtenstein, and R. A. de Groot, Rev. Mod. Phys. **80**, 315 (2008).
[13]I. Žutic, J. Fabian, and S. D. Sarma, Rev. Mod. Phys. **76**, 323 (2004).
[14]H. van Leuken and R. A. de Groot, Phys. Rev. Lett. **74**, 1171 (1995).
[15]P. Blaha, K. Schwarz, G. Madsen, D. Kvasnicka, and J. Luitz, *WIEN2k, An Augmented Plane Wave Plus Local Orbitals Program for Calculating Crystal Properties* (Vienna University of Technology Inst. of Physical and Theoretical, Vienna, Austria, 2008); P. Blaha, K. Schwarz, and P. Sorantin, Comput. Phys. Commun. **59**, 399 (1990).
[16]J. Kudrnovský and V. Drchal, Phys. Rev. B **41**, 7515 (1990).
[17]I. Turek, V. Drchal, J. Kudrnovský, M. Šob, and P. Weinberger, *Electronic Structure of Disordered Alloys, Surfaces and Interfaces* (Kluwer, Boston-London-Dordrecht, 1997).
[18]P. Hohenberg and W. Kohn, Phys. Rev. **136**, B864 (1964); W. Kohn and L. J. Sham, Phys. Rev. **140**, A1133 (1965).
[19]J. P. Perdew, K. Burke, and M. Ernzerhof, Phys. Rev. Lett. **77**, 3865 (1996).
[20]H. J. Monkhorst and J. D. Park, Phys. Rev. B **13**, 5188 (1976).
[21]S. H. Vosko, L. Wilk, and M. Nusair, Can. J. Phys. **58**, 1200 (1980).
[22]F. D. Murnaghan, Proc. Natl. Acad. Sci. U.S.A. **30**, 244 (1944).
[23]L. M. Sandratskii, R. Singer, and E. Sasioğlu, Phys. Rev. B **76**, 184406 (2007).
[24]M. Pajda, J. Kudrnovský, I. Turek, V. Drchal, and P. Bruno, Phys. Rev. B **64**, 174402 (2001).
[25]S. K. Bose and J. Kudrnovský, Phys. Rev. B **81**, 054446 (2010).
[26]Y. Liu, S. K. Bose, and J. Kudrnovský, Phys. Rev. B **82**, 094435 (2010).
[27]A. I. Liechtenstein, M. I. Katsnelson, and V. A. Gubanov, J. Phys. F: Met. Phys. **14**, L125 (1984).
[28]A. I. Liechtenstein, M. I. Katsnelson, and V. A. Gubanov, Solid State Commun. **54**, 327 (1985).
[29]V. A. Gubanov, A. I. Liechtenstein, and A. V. Postnikov, *Magnetism and the Electronic Structure of Crystals*, edited by M. Cardona, P. Fulde, K. von Klitzing, and H.-J. Queisser (Springer, Berlin, 1992).
[30]I. Turek, J. Kudrnovský, V. Drchal, and P. Bruno, Philos. Mag. **86**, 1713 (2006).
[31]V. Heine, J. H. Samson, and C. M. M. Nex, J. Phys. F: Met. Phys. **11**, 2645 (1981).
[32]V. Heine and J. H. Samson, J. Phys. F: Met. Phys. **13**, 2155 (1983).
[33]W.-Z. Wang and X.-P. Wei, Comput. Mater. Sci. **50**, 2253 (2011).
[34]I. Galanakis, K. Özdoğan, E. Sasioğlu, and B. Aktaş, Phys. Rev. B **75**, 172405 (2007).
[35]I. Galanakis, K. Özdoğan, E. Sasioğlu, and B. Aktaş, Phys. Rev. B **75**, 092407 (2007).
[36]Yung -mau Nie and X. Hu, Phys. Rev. Lett. **100**, 117203 (2008).
[37]M. Nakao, Phys. Rev. B **74**, 172404 (2006).
[38]C. S. Wang, R. E. Prange, and V. Korenman, Phys. Rev. B **25**, 5766 (1982).
[39]L. Bergqvist, O. Eriksson, J. Kudrnovský, V. Drchal, P. Korzhavyi, and I. Turek, Phys. Rev. Lett. **93**, 137202 (2004).
[40]K. Sato, W. Schweika, P. H. Dederichs, and H. Katayama-Yoshida, Phys. Rev. B **70**, 201202(R) (2004).
[41]G. Bouzerar, T. Ziman, and J. Kudrnovský, Europhys. Lett. **69**, 812 (2005).
[42]K. Carva, I. Turek, J. Kudrnovský, and O. Bengone, Phys. Rev. B **73**, 144421 (2006).
[43]I. Turek, J. Kudrnovský, V. Drchal, L. Szunyogh, and P. Weinberger, Phys. Rev. B **65**, 125101 (2002).
[44]J. M. Ziman, *Electrons and Phonons* (Oxford University Press, Oxford, 1960).
[45]Y. Liu, S. K. Bose, and J. Kudrnovský, J. Appl. Phys. **112**, 053902 (2012).